VERSITA

Acta Geophysica
vol. 60, no. 3, Jun. 2012, pp. 769-793
DOI: 10.2478/s11600-012-0036-6

Ergodicity Examined by the Thirumalai–Mountain Metric for Taiwanese Seismicity

Hsien-Chi LI and Chien-Chih CHEN

Department of Earth Sciences and Institute of Geophysics,
National Central University, Jhongli, Taiwan
e-mail: chencc@earth.ncu.edu.tw (corresponding author)

Abstract

Ergodicity is a behavior generally limited to equilibrium states and is here defined as the equivalence of ensemble and temporal averages. In recent years, effective ergodicity is identified in simulated earthquakes generated by numerical fault models and in real seismicity of natural fault networks by using the Thirumalai–Mountain metric. Although the effective ergodicity is already reported for Taiwanese seismicity, an immediate doubt is the unrealistic gridded sizes for discretizing the seismic data. In this study, we re-examined the effective ergodicity in Taiwanese seismicity by using reasonable gridded sizes which corresponded with the location errors in the real earthquake catalogue. Initial time and magnitude cut-off were examined for the validity of ergodic behavior. We found that several subsets extracted from Taiwanese seismicity possessed effectively ergodic intervals and all terminations of these ergodic intervals temporally coincided with the occurrences of large earthquakes ($M_L < 6.5$). We thus confirm the ergodicity in the crustal seismicity by using the Thirumalai–Mountain metric.

Key-words: ergodicity, Thirumalai–Mountain metric, seismicity, Taiwan.

1. INTRODUCTION

Ergodicity is a behavior generally limited to equilibrium states in physical systems. Although the definition of ergodicity varies with the contents studied, we here define the ergodicity as the equivalence of ensemble and temporal averages. A necessary condition of ergodicity is thus the statistical stationarity for a physical system. Practically, if the actual measurement time is finite but long enough, most of the accessible phase space for the system will be equally likely sampled; thus, the system is ***effectively ergodic***. The Thirumalai–Mountain (TM) metric, which is usually used in material science, is originally developed to examine the time scale to obtain ergodicity in numerical models of liquids, supercooled liquids, glasses and so forth (Thirumalai *et al.* 1989). The TM metric, $\Omega_e(t)$, which is related to the time-averaged energy of individual sites, is used to measure the effective ergodicity by calculating the difference between the temporal average of a specific quantity at each site and its ensemble average over the entire system. Once the system is identified as effectively ergodic over an interval, the spatial statistics of the system maintain stationarity. Furthermore, a dynamical scaling law of $\Omega_e(t)$ then furthermore characterizes the behavior of effective ergodicity.

In recent years, earthquake fault networks are viewed as a subset of natural nonlinear, driven threshold systems (Scholz 1990, Rundle and Klein 1995, Fisher *et al.* 1997). Other examples of such systems include neural networks (Hertz *et al*. 1991, Herz and Hopfield 1995), depinning transitions in charge-density waves and superconductors (Fisher 1985), magnetized domains in ferromagnets (Urbach *et al.* 1995), sand-piles (Bak *et al.* 1987), and foams (Gopal and Durian 1995). For seismic fault networks, effective ergodicity is first identified while the TM metric is applied to analyze the simulated seismicity generated by numerical fault models with nonlinear parameters (Ferguson *et al.* 1999, Klein *et al.* 1997). In the scenario developed from the analyses of fault models, small to moderate earthquakes are treated as fluctuations of a system in thermal equilibrium. On the other hand, occurrence of large earthquakes drives the system out of existing equilibrium state and results in the destruction of ergodicity (Chen *et al.* 2008, Lee *et al.* 2008). The effective ergodicity in natural seismic catalogues has already been reported in several regions with different tectonics, such as California, eastern Canada, Spain, and Taiwan (Tiampo *et al*. 2003, 2007, 2010). All of the fault systems display punctuated ergodic behaviors in several intervals while various combinations of magnitude cut-off and spatial gridding are used in Tiampo *et al.* (2003, 2007, 2010).

Although the effective ergodicity has already been reported for Taiwanese seismicity by Tiampo *et al.* (2010), an immediate doubt is the unrealistic

application of gridded size for discretizing the seismic data. For example, the side length of two-dimensional planar box is 0.02° and the depth discretization of three-dimensional rectangular box is even as small as 0.25 km in Tiampo *et al*. (2010). Obviously, these length scales are unrealistically small considering the location quality in real earthquake catalogue like Taiwanese Central Weather Bureau Seismometer Network (TCWBSN). We wonder if unrealistic small discretization could induce an artificial ergodicity as identified in the early study due to the noises of earthquake location.

In Tiampo *et al.* (2010), the data used is 1973-2009 and the authors are forced to apply too small gridding box to search for possible effective ergodicity. However, we find that once the earlier data is excluded, effective ergodicity exists using various, statistical reasonable, grid sizes. The influence about catalogue quality is never evaluated in detail in previous researches about effective ergodicity of natural catalogues. Our research shows crucial influence of heterogeneity in the CWBSN catalogue on effective ergodicity evaluated by TM metric. In this paper we adopt statistically reasonable gridded sizes, all of which corresponded to the tolerance of seismic location quality, instead of unrealistic applications in previous research to search for possible effectively ergodic behaviors in the Taiwanese seismicity. Initial time and magnitude cut-off are chosen to define various subsets of the TCWBSN catalogue. Each subset of earthquake data is divided spatiotemporally and then utilized to calculate the TM metric. We examine whether effective ergodicity exists in these subsets by evaluating their TM metrics. We find that several subsets of TCWBSN catalogue possess effectively ergodic intervals indeed. Furthermore, all terminations of identified ergodic intervals are temporally related to the occurrences of large earthquake. The existence of effective ergodicity in Taiwanese seismicity reveals the possibility of applying forecasting algorithms based on statistical stationary of seismicity (*e.g*., Chen *et al*. 2005, 2006). For example, correct seismic anomalies evaluated by pattern informatics (PI) crucially depend on stationary spatial variance of long-term average seismic rate (Rundle *et al.* 2002, Tiampo *et al*. 2002). The determination of effective ergodicity can provide crucial parameters to decompose seismic data into many segments having statistical stationarity.

2. SEISMICITY DATA

The primary seismicity dataset for Taiwan and nearby islands used in this study is the earthquake catalogue released from the Central Weather Bureau, Taiwan. The seismic history of instrumental observation was initiated in 1896, when the Japanese government set up the first seismometer in Taipei. By 1941 there were a total of fourteen seismometers installed on the Taiwan

Island. This seismic observation network was then furthermore upgraded to the electromagnetic instruments by the Taiwanese Central Weather Bureau (CWB). At the same time, the coverage of seismic network was also improved by establishing more observation stations. A seismology group (the predecessor of the Institute of Earth Sciences) based on the Academia Sinica, Taipei, Taiwan, began to set up the first modern telemetered monitoring network in 1972. That telemetered seismic network with twenty five stations significantly improved the location precision of hypocenters and the detection ability for small earthquakes. Teleseismic network of the Institute of Earth Sciences, Academia Sinica, was eventually combined with the original CWB seismic network (CWBSN) in 1991 as a new real-time digital observation network. In 1993, the CWBSN instruments were upgraded to the continuous recording mode, instead of the triggered recording mode. Arrival times of *P* and *S* waves are then manually picked for determining epicenter location and Richter local magnitude (M_L). Therefore, available modern record of Taiwanese seismicity can be traced back from 1973. We use the dataset of modern Taiwanese seismic catalogue from 1973 through 2009 in this study.

We introduced several important characteristics of Taiwanese seismicity in Fig. 1. Figure 1a shows the distribution of cumulative ratio of earthquake number above various depth thresholds. The seismic data was selected to locate between 119° to 123° longitude, and 21° to 26° latitude, and no magnitude threshold was used. The seismic data was separated into three intervals, 1973-1983, 1984-1990, and 1991-2009, by referring to important improvements of seismometer network. Total numbers of earthquake in each interval are 46187, 44421, and 350036, respectively. The x value indicates depth threshold, D_c, and continuously changes from 100 km underground to ground surface (0 km) in application. Cumulative number of earthquakes was the number of earthquakes whose focal depths locate in the depth range from ground surface to D_c [km]. The y axis indicates the ratio of cumulative earthquake number and was obtained by dividing cumulative numbers of earthquakes by the total earthquake number in the corresponding interval. Black, gray, and light gray curves indicate the seismic data of 1973-1983, 1984-1990, and 1991-2009, respectively. The distribution curves of 1973-1983 and 1984-1990 show that 80 percent of earthquakes occurred above 30 km, and 90 percent of earthquakes occurred above 40 km. The curve of 1991-2009 shows that 80 percent of earthquakes occurred above 20 km, and 90 percent of earthquakes occurred above 30 km. There are merely 10 percent of earthquakes in the range of 40-100 km. Figure 1a reveals that most earthquakes in Taiwan occurred in a very thin depth range from ground surface to 30 km underground. This characteristic motivated us to use 30 km as a proper depth threshold.

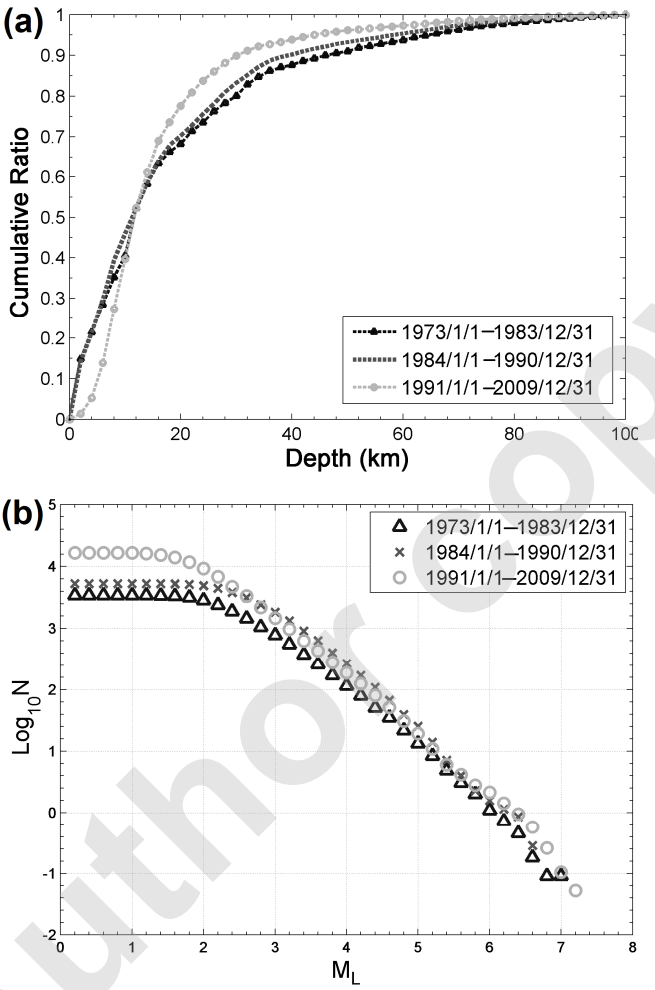

Fig. 1: (a) Distribution of cumulative ratio of earthquake number above successive depth thresholds in Taiwan. Black, gray, and light gray curves indicate the seismic data of 1973-1983, 1984-1990, and 1991-2009. (b) Gutenberg–Richter frequency distributions of seismic data in Fig. 1a. The *x* value indicates magnitude which continuously changed from 8.0 to 1.0. Yearly seismic rate for a specific cut-off magnitude is defined as the total number of earthquakes ($\geqq M$) divided by the number of years in an interval and expressed on logarithmic scale.

The Gutenberg–Richter frequency distributions for seismic data above 30 km in focal depth are displayed in Fig. 1b. The seismic data are separated into three intervals in the same way as in Fig. 1a. According to the definition of the Gutenberg–Richter (GR) law (Gutenberg and Richter 1954), the *x* value indicates magnitude and continuously changes from 8.0 to 1.0 in our

application. Yearly seismic rate of a specific magnitude in an interval was defined by dividing the total number of earthquakes with magnitudes equal to or greater than this magnitude by number of years. For a specific magnitude, the corresponding y value was obtained by expressing yearly seismic rate on a logarithmic scale. Based on the curves in Fig. 1b, there are yearly 90, 205, and 162 earthquakes whose magnitudes are equal to or greater than 3.0 in 1973-1983, 1984-1990, and 1991-2009. Unlike linear patterns of other two curves at magnitude 2.5 to 3.8, there is an interesting bulge of the curve for 1984-1990. Referring to corresponding seismic data, we found that only the seismicity in 1986 was much higher than in other years of the period 1984-1990. Thus we suggest that this bulge of GR law curve was caused by the aftershocks due to four large earthquakes in 1986. On the other hand, there is also a bulge of GR law curve in 1991-2009 at a magnitude greater than 5.0. We found that only the seismicity of magnitude greater than 4.0 in 1999 was several times the intensity of other years in the 1991-2009 period and thus contributed to this bulge with the enormous aftershocks created by the 1999 Chichi earthquake.

Wu *et al*. (2008) analyzed the spatial distribution of completeness magnitude for the CWBSN catalogue using the data from 1994 to 9 October 2003 and 35 km as the depth threshold. They show that the completeness magnitude is 2.2 for on-land events and even reaches 1.2 in several metropolises. On the other hand, the completeness magnitude ranges from 2.5 to 3.0 for offshore events. Also, Mignan *et al.* (2011) used the data from 1994 to March 2010 shallower than 35 km and concluded that the completeness magnitude is 2.0 for most of the Taiwan Island region and is 2.4 for the coast region. In Telesca *et al.* (2009), the completeness magnitude is determined to be 2.0 by using data from 1990 to 2007 and 30 km as depth threshold. In Tsai *et al*. (2011), the CWBSN catalogue can be divided into six time-periods with different stable M_c according to the fluctuations of completeness magnitude, which are: (i) 1973-1978 ($M_c = 2.7$), (ii) 1978-1986 ($M_c = 2.8$), (iii) 1986-1994 ($M_c = 3.2$), (iv) 1994-2002 ($M_c = 2.3$), (v) 2002-2008 ($M_c = 2.2$), and (vi) 2008-2010 ($M_c = 2.1$). We also applied the freely available tool ZMAP (Wiemer 2001) to analyze the completeness magnitude corresponding to each interval in Fig. 1a. Using the maximum curvature method (MAXC; Wiemer and Wyss 2000) and the entire-magnitude-range method (EMR; Ogata and Katsura 1993), the completeness magnitudes are 2.1, 2.6, 2.0, and 2.4, 2.7, 2.1 for the intervals of 1973-1983, 1984-1990, and 1991-2009, respectively. The values of completeness magnitude for the shallower seismicity after 1994 are quite consistent in those studies addressed above and our analysis. Furthermore, the larger completeness magnitude for 1984-1990 corresponds with the pattern of frequency-magnitude curve observed in Fig. 1a.

3. THIRUMALAI–MOUNTAIN FLUCTUATION METRIC

For a seismic fault network, the parameter $E_i(t')$ is a quantity which is the energy or a proxy of the energy of an individual site at time t'. For each individual box i in a system, let

$$\varepsilon_i(t) = \frac{1}{t}\int_0^t E_i(t')\mathrm{d}t' \tag{1}$$

be the time average of E_i over an interval. If there are N boxes in the seismic fault network, the ensemble average is obtained by averaging the temporal average rates, evaluated in the same interval, over all boxes,

$$\overline{\varepsilon}(t) = \frac{1}{N}\sum_{i=1}^{N}\varepsilon_i(t)\,. \tag{2}$$

To evaluate the difference between the temporal mean and the ensemble mean, a TM metric is introduced as

$$\Omega_e(t) = \frac{1}{N}\sum_{i=1}^{N}\left[\varepsilon_i(t) - \overline{\varepsilon}(t)\right]^2. \tag{3}$$

In fact, this measure is the spatial variance of the temporal averages. If the system is ergodic on the time scale τ_{obs}, the measure $\Omega_e(t)$ should vanish as t approaches τ_{obs} due to the rapid and uniform sampling of all allowed phase space. On the other hand, when ergodicity is broken, the measure $\Omega_e(t)$ should approach a nonzero constant as t approaches τ_{obs}.

Thirumalai *et al*. (1989) deduced a dynamical scaling law to describe the finite-time properties of ergodicity from their numerical simulations of liquid model. The scaling law reveals that, for an effectively ergodic system, the reciprocal of the spatial variance grows linearly with time, just like the following equation:

$$\frac{\Omega_e(0)}{\Omega_e(t)} = \frac{t}{D_e}\,. \tag{4}$$

The denominator, $\Omega_e(0)$, in Eq. (4) is the TM measure at initial time t which equals zero. The constant parameter D_e is related to the exploration rate of the phase space and can be used to estimate the time required to make a system attain ergodicity. This scaling behavior is suggested to relate to the central limit theorem, where the variance becomes a constant controlled by the large sample size N and is divided by the increasing time t.

In applying the TM metric to analyze real seismic catalogue, the number of earthquake is adopted as a proxy for seismic energy release (Tiampo *et al*. 2007). The research region ranged from 21° to 26° latitude and from 119° to

123° longitude. Several factors, such as moving time step of t in Eq. (1), dimensionality and size of dividing box, and cut-off magnitude, were tested to define possible effective-ergodic intervals in the CWB catalogue at which the statistical distribution of long term average seismic rates remained stationary. Referring to Fig. 1a, we used the seismic data whose focal depths were above 30 km in order to focus on the behavior of seismicity in shallower depths. Furthermore, we adapted both two- and three-dimensional boxes to divide the same seismic data set in space to reveal the depth effect of the CWB catalogue in TM metric calculation. For each inverse TM metric figure, the values of inverse TM metric at every time step were divided by the value of the first time step in each analysis, for example: 1-30 January 1973 while the unit time step is 30 days, to produce the normalized values. Besides several factors addressed above, we also noticed possible influence induced by the combination of the seismic networks and by the upgrade of seismometers on quality of earthquake location.

4. RESULTS OF NORMALIZED INVERSE TM METRIC

4.1 Cut-off magnitude of 2.5

Referring to the Gutenberg–Richter frequency distributions in Fig. 1b, the completeness of CWBSN catalogue can extend to magnitude 2.5. Thus we used 2.5 as a magnitude cut-off to compose earthquake data set. Figure 2 shows the results of normalized inverse TM metric using 30 days as unit time step. Based on the record of seismic location quality, the average of standard error of focal location in epicenter and depth is 1.84 and 2.79 km, respectively, during 1973-2009. For the earlier data, during 1973-1986, the average of standard error of focal location in epicenter and depth increases to 3.27 and 5.82 km, respectively. Thus we applied a reasonable two-dimensional square dividing box which was 0.1° in side length to easily overcome the error of epicenter location.

Figure 2a shows the result of normalized inverse TM metric, the data of which began in January 1973. Two thicker arrows in Fig. 2a, respectively, indicate the time points of two major evolutions of CWBSN, *i.e.*, upgrade to electromagnetic instruments since 1984 and the combination of IES and original CWB networks in 1991. The bars extending vertically from the time axis of Fig. 2a indicate the big earthquakes which are greater than or equal to 6.0 in magnitude from 1973 to 2009. The value of normalized inverse TM metric is very large and fluctuates apparently while the parameter t is moving from 1973 to June 1978, drops dramatically in 1978 and then gradually decreases in 1979 to 1986. Finally, the normalized inverse TM metric value remains stable around 0.25 after 1987.

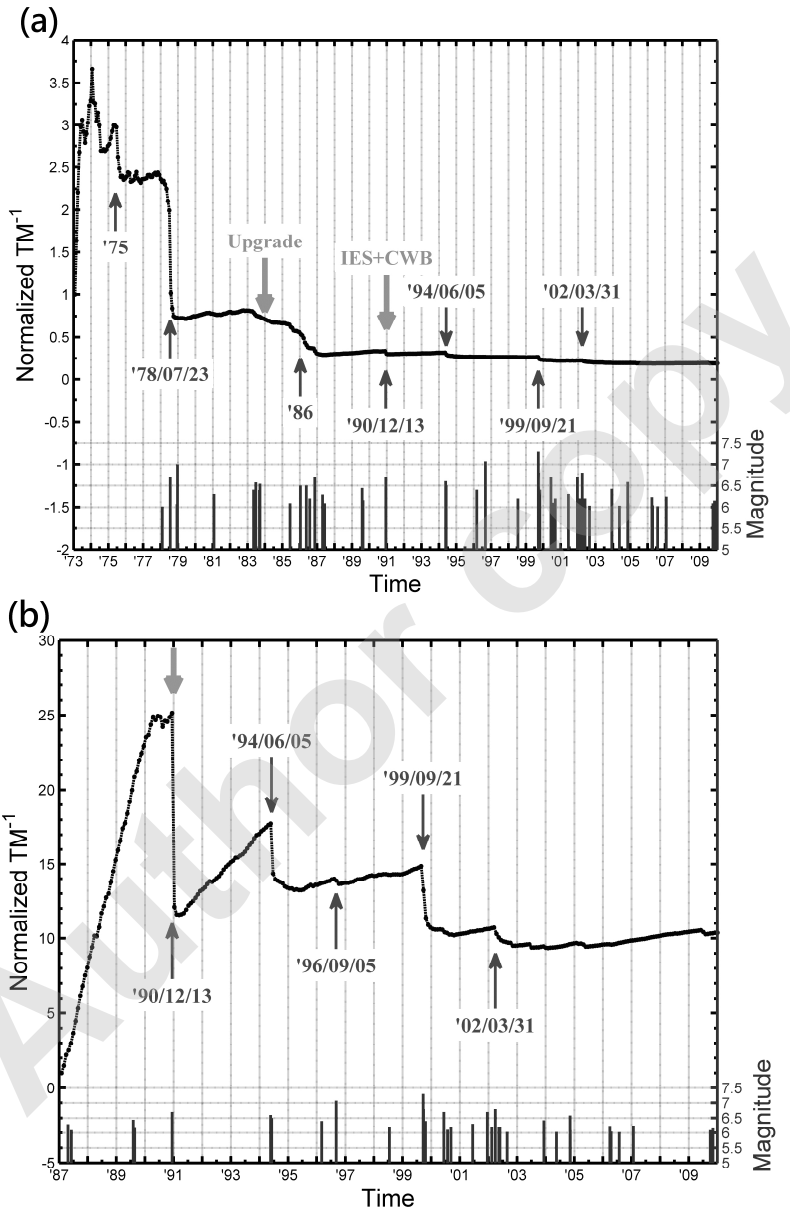

Fig. 2. Normalized inverse TM metric for Taiwan, two-dimensional box size equal to 0.1° × 0.1°, $M \geqq 2.5$, and $D_c = 30$ km. Vertical bar indicates the occurrence time of $M \geqq 6.0$ earthquakes. Thicker arrow indicates the time point of major evolutions of CWBSN. Upgrade: upgrade to electromagnetic instruments, IES+CWB: combination of IES network and original CWB network. Study period is (a) 1973-2009; (b) 1987-2009.

Although the pattern of normalized inverse TM metric curve in Fig. 2a is far from the required linear pattern of effective ergodicity, we identified apparent influence of large earthquakes on three large drops of normalized TM metric. In 1975, there was a series of earthquakes whose magnitude ranged from 5 to 6. On 23 July 1978, there was a big earthquake of 6.7 magnitude. In 1986, there were four big earthquakes whose magnitudes ranged from 6.2 to 6.7. Besides these large drops, we also identified four smaller drops of normalized inverse TM metric in December 1990, June 1994, September 1999, and March 2002. All of the smaller drops are correlated with the occurrences of large earthquake, including the 1999 Chichi earthquake and the 2002 Hualian earthquake.

Considering the quite different patterns of normalized inverse TM metric between 1973 to 1986 and 1987 to 2009 in Fig. 2a, we adopted 1987 as another beginning to remove an influence due to heterogeneity of earlier data in CWB catalogue and Fig. 2b shows the result. The thick arrow indicates the time point of combination of IES and original CWB networks since 1991. We identified three large drops of normalized inverse TM metric in December 1990, June 1994, and September 1999. All of them are temporally correlated with the occurrences of a big earthquake whose magnitude is greater than 6.5.

We also identified three intervals as candidates for an effectively ergodic interval, *i.e.*, January 1987 to April 1990, June 1991 to April 1994, and November 1996 to August 1999. The linear regression models for each interval are obtained by least-square fitting and the slopes of each regression model are 0.627, 0.158, and 0.029, respectively.

4.2 Cut-off magnitude of 3.0

We tested another data set whose cut-off magnitude was 3.0. Based on the record of data quality from 1973 to 2009, the average of standard error of focal location in epicenter and depth was, respectively, 1.81 and 2.4 km. For the earlier data from 1973 to 1986, poorer location quality raised the average of standard error of focal location in the epicenter and depth to 4.43 and 7.83 km, respectively. Thus, we still applied two-dimensional square dividing boxes, whose side length was 0.1° to overcome the error of epicenter location.

The pattern of normalized inverse TM metric in Fig. 3a is very similar to the curve in Fig. 2a. Two large drops in 1975 and 1978 are the same as those in Fig. 2a, but the drops in 1986 become steeper. Figure 3b-c shows the normalized inverse TM metric results using seismic data since 1987. Based on the record of data quality in 1987 to 2009, the average standard error of focal location in epicenter and depth was 1.2 and 1.45 km, respectively. We used two-dimensional square gridding box whose side length was 0.1° in

Fig. 3b and three-dimensional gridding box whose size was 0.1° × 0.1° × 3 km in Fig. 3c.

The patterns of normalized inverse TM metric in Fig. 3b-c are quite different from that in Fig. 3a. Both inverse TM metric curves in Fig. 3b-c show several linearly increasing patterns which are terminated by drops. We

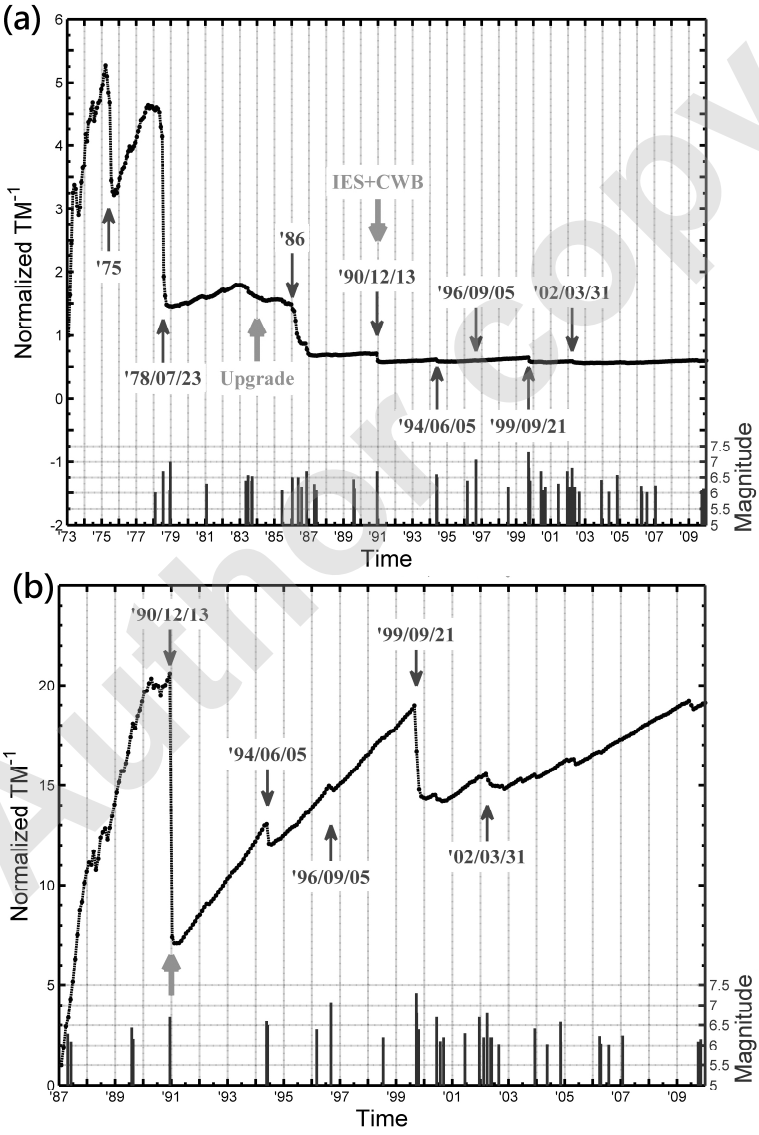

Fig. 3. Continued on next page.

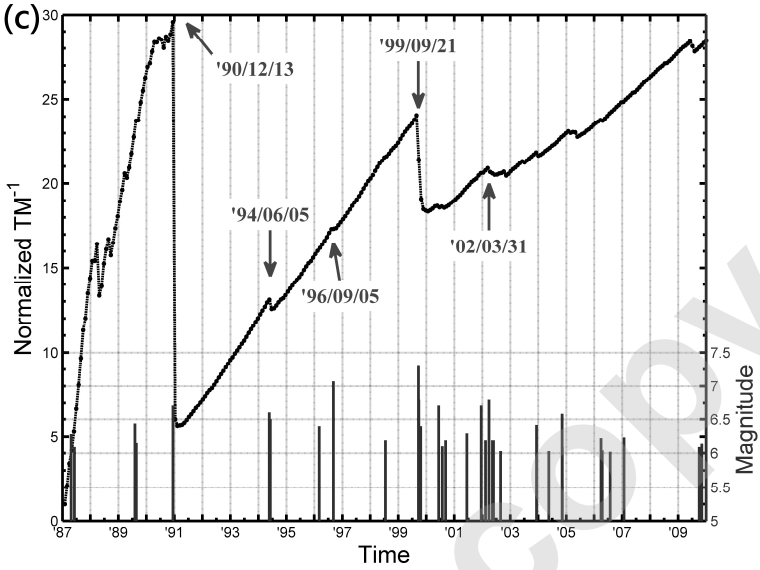

Fig. 3. Normalized inverse TM metric for Taiwan, $M \geqq 3.0$, and $D_c = 30$ km. Box size is 0.1° × 0.1° in (a) and (b); 0.1° × 0.1° × 3 km in (c). Study period is 1973-2009 in (a); 1987-2009 in (b) and (c).

identified four big drops in December 1990, June 1994, September 1996, and September 1999, and three possible effectively ergodic intervals between the drops in Fig. 3b. All drops are closely correlated to the occurrences of big earthquake whose magnitude exceeds or equals 6.5. We also identified two possible effectively ergodic intervals, from September 2000 to February 2002 and from June 2005 to June 2009.

Furthermore, we found that the magnitude of normalized inverse TM metric drops in June 1994 and September 1996 in Fig. 3b are larger than those in Fig. 3c. The values of inverse TM metric which change in June 1994 and September 1996 in Fig. 3b are –1 and –0.2, being –0.55 and 0.2 in Fig. 3c. This disappearance of drop in September 1996 in Fig. 3c was caused by the enormous increase of the number of three-dimensional dividing boxes. The significantly increasing number of dividing boxes strongly reduced the influences of seismic data at a next time step and maintained the statistical distribution of long-term average seismic rate stable.

Similar to Section 4.1, we obtained linear regression models of each possible effectively ergodic interval by least-square fitting. Five candidates of effectively ergodic intervals are: June 1991 to May 1994, August 1994 to August 1996, November 1996 to August 1999, September 2000 to February 2002, and June 2005 to June 2009. The corresponding slopes are 0.154,

0.117, 0.119, 0.078, and 0.066 in Fig. 3b, and 0.199, 0.181, 0.191, 0.131, and 0.118 in Fig. 3c.

4.3 Cut-off magnitudes of 4.0 and 5.0

Figure 4a-b shows the results of normalized inverse TM metric using seismic data which exceed or equal 4.0 in magnitude. In both cases we discretized

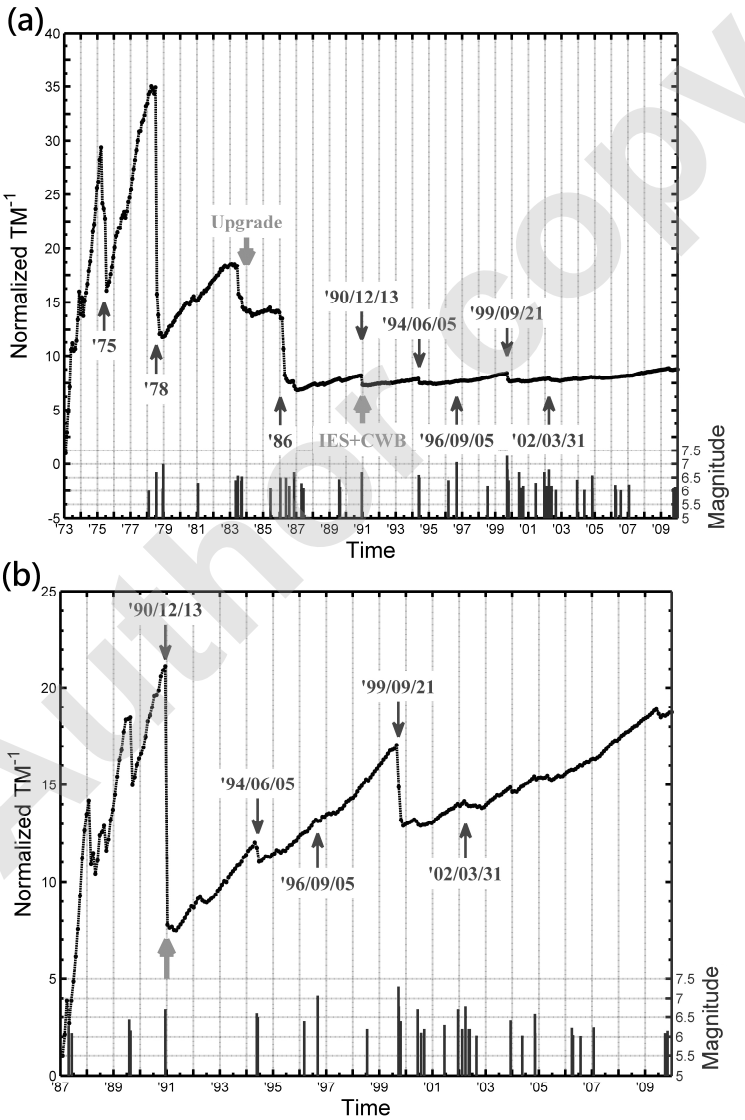

Fig. 4. Continued on next page.

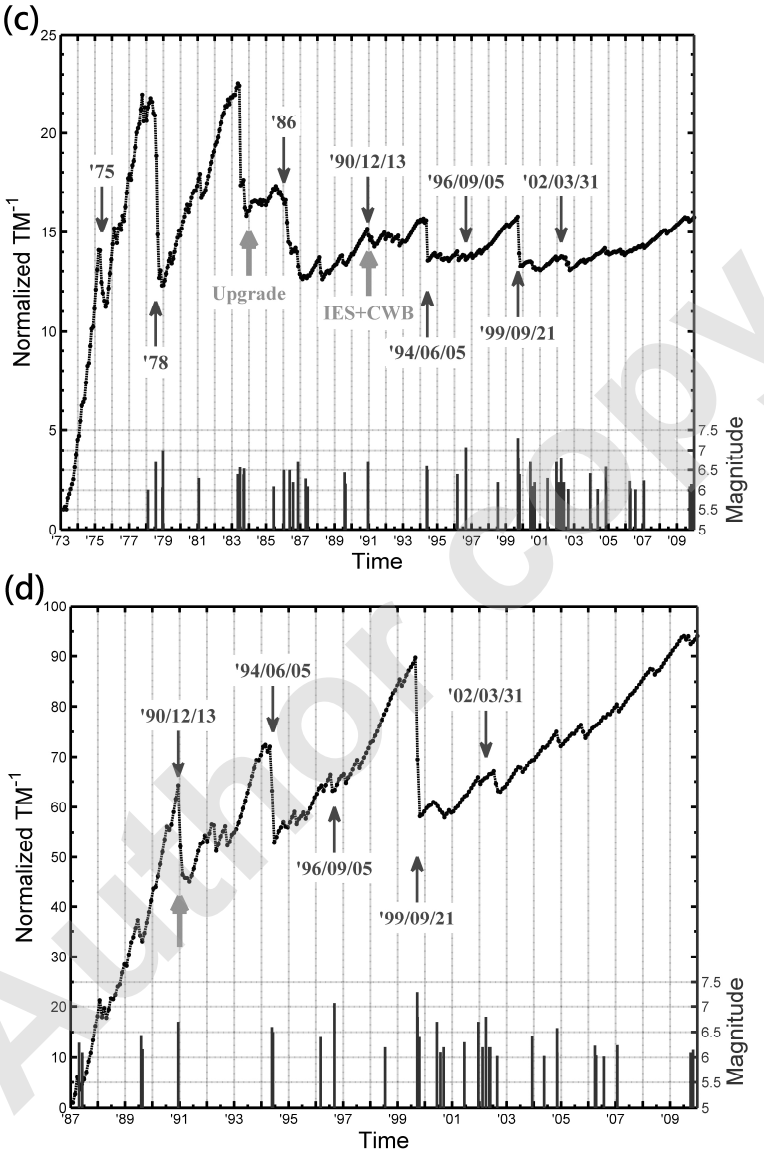

Fig. 4. Normalized inverse TM metric for Taiwan, two dimensional box size is equal $0.1° \times 0.1°$, $D_c = 30$ km. $M \geqq 4.0$ for (a) and (b); $M \geqq 5.0$ for (c) and (d). Study period is 1973-2009 for (a) and (c); 1987-2009 for (b) and (d).

the data set by using thirty days as the unit time step and two-dimensional square dividing box whose side length was 0.1°. The only difference between Fig. 4a and b is the initial time of seismic data set. The data initi-

ated, respectively, from January 1973 in Fig. 4a and from January 1987 in Fig. 4b. Similar to Figs. 2a and 3a, the normalized inverse TM metric curve fluctuates strongly before 1987 in Fig. 4a. The pattern of normalized inverse TM metric in Fig. 4b is similar to Fig. 3b-c. We observed new drops of inverse TM metric in April 1992 to June 1992, which did not exist in the analyses using smaller magnitude cut-off. Comparing to the seismic catalogue, there is a series of shallow earthquakes whose magnitude ranged from 5.0 to 5.6. We also observed that the inverse TM metric in September 1996 formed a bulge instead of a drop. We suggested that the application of 4.0 as a magnitude cut-off eliminated the influence of smaller aftershocks which were generated by the Lanyu earthquake on 5 September 1996.

We identify two candidates of effectively ergodic interval, June 1991 to April 1992 and August 1992 to April 1994, from Fig. 4b. Another interval, from July 1994 to August 1999, in which the inverse normalized TM metric fluctuates stronger, is also tested. The slopes are 0.159, 0.143, and 0.095, respectively.

Figure 4c-d shows the results of normalized inverse TM metric using 5.0 as magnitude cut-off. The initial time of seismic data is January 1973 in Fig. 4c and January 1987 in Fig. 4d. The impact of using earlier seismic data, before 1987, is still obvious in Fig. 4c. Comparing to Figs. 3b-c and 4b, the magnitudes of inverse normalized TM metric do not raise very rapidly in 1973 to 1986. On the other hand, the inverse TM metric curve in January 1991 to May 1994 and June 1994 to August 1999 fluctuates more apparently than in Figs. 3b-c, and 4b. We suggest that the earthquakes whose magnitude is greater than 5.0 are too few to construct a stable statistical distribution of long-term average seismic rate. The statistical distribution of long term average seismic rate is easily affected by the number of earthquake at a following time step.

5. DISCUSSION

The evolution of detecting ability and coverage of CWBSN must have caused the statistical properties of seismicity to be different in varying time points. For example, an evaluation of homogeneity in the CWBSN catalogue shows significant rate increases until pre-1980 and the rate anomalies corresponding to large earthquake sequences (Habermann 1987, Tiampo *et al*. 2010). Figure 1 specifically illustrates different statistical properties of seismicity due to the evolutions of CWBSN. In Figures 2a, 3a, and 4a, we identified apparent influences of using earlier data, before 1987, in the calculation of inverse TM metric. Conversely, obvious linearly increasing patterns of inverse normalized TM metric curves exist in the analyses disregarding the earlier data. However, even in Figs. 3b-c, and 4b, the abrupt raise and relatively larger fluctuations of inverse TM curve in 1987 to 1990

still implied the influences of heterogeneity in seismic data. In further tests, not shown in this paper, which used January 1991 as the initial time, there is no such large fluctuation of inverse TM metric in the beginning interval. We suggested that this change is due to more stable detecting ability of CWBSN since 1991. These tests about heterogeneity of catalogue reveal the necessity of carefully considering possible bias of long term seismic rate while earlier seismic data is involved.

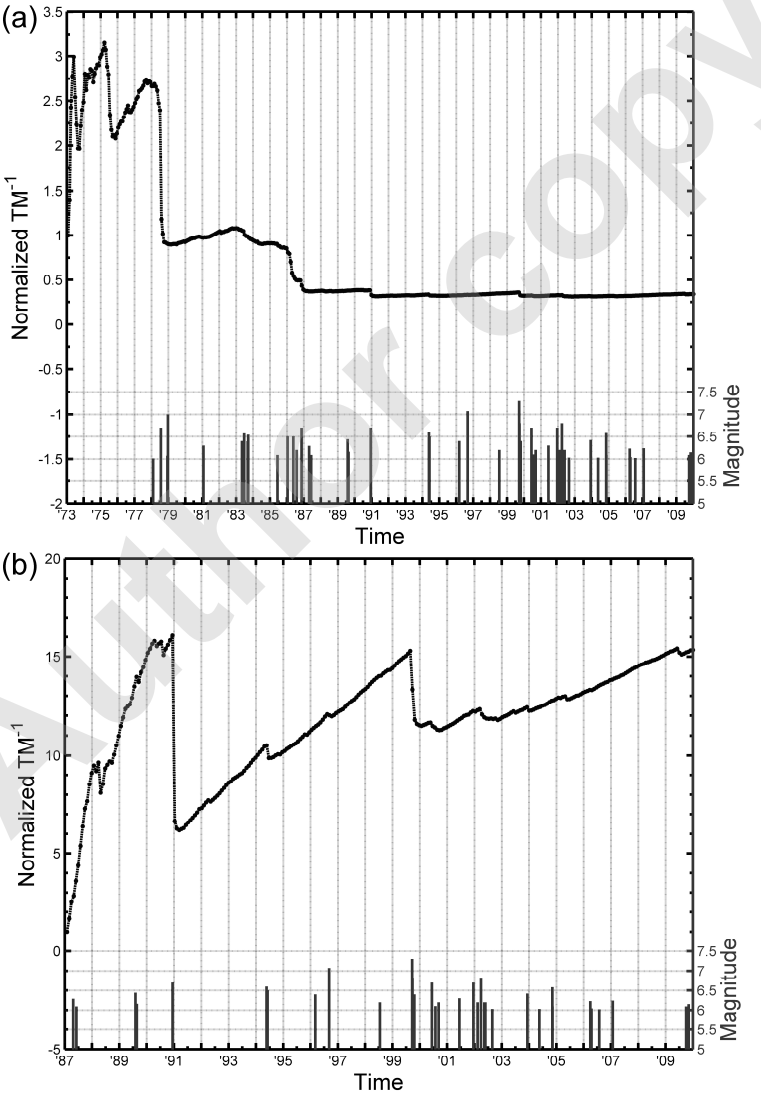

Fig. 5. Continued on next page.

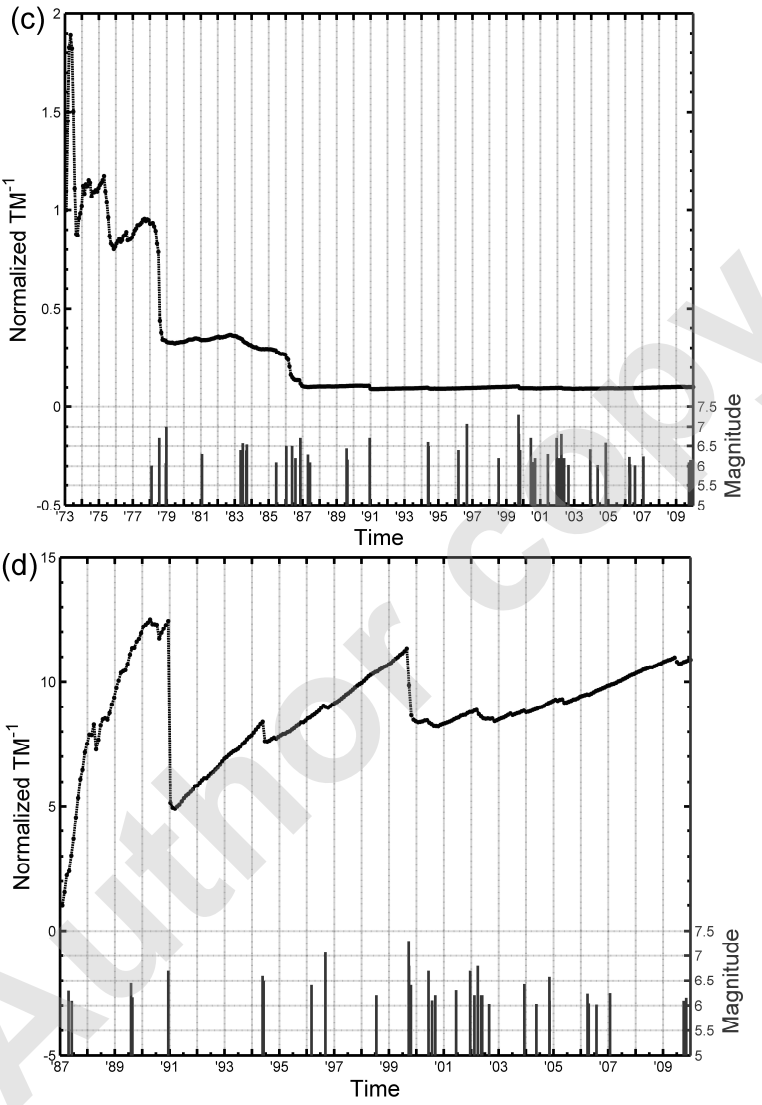

Fig. 5. Normalized inverse TM metric for Taiwan, $M \geqq 3.0$, and $D_c = 30$ km. Box size is 0.2° × 0.2° in (a) and (b); 0.1° × 0.5° in (c) and (d). Study period is 1973-2009 in (a) and (c) as a comparison to Fig. 3a; 1987-2009 in (b) and (d) as a comparison to Fig. 3b.

Through the results in Figs. 2b, 3b and d, and 4b, we identified several intervals in which the inverse normalized TM metric curves had linearly increasing patterns. According to the somewhat obscure dynamical law

addressed in the method section, the Taiwanese fault network might be regarded as being effectively ergodic in these intervals. However, more quantitative analyses are necessary for finding further details of the candidates of effective ergodicity. First, are these linearly increasing patterns originated from the nature of Taiwanese seismicity or merely obtained occasionally due to application of a specific gridding box? Second, if these effectively ergodic intervals exist in nature, is there any common characteristic among them?

We tested the possible influence of gridding box size by using larger grid to discretize the data sets used in Fig. 3a-b, and illustrated the inverse TM metric results in Fig. 5. The side length of two-dimensional square gridding box is 0.2° in Fig. 5a-b, and 0.5° in Fig. 5c-d. The initial time is January 1973 in Fig. 5a and c, the same as in Fig. 3a, and January 1987 in Fig. 5b, d, the same as in Fig. 3b. An immediate observation is that the curve patterns are highly similar among the results using the same data set. These results show that the size of gridding box does not alter the behavior of inverse TM metric curve obviously. The linearly increasing patterns of inverse TM metric curve observed in Fig. 3b still exist in Fig. 5c-d. Thus we conclude that the existence of possible effective ergodicity crucially depends on the inherent properties, *e.g.*, heterogeneity, of data set used. The linearly increasing patterns of inverse TM metric curve in Fig. 3b exist naturally; they are not an artificial effect using a specific gridding box.

In order to further understand properties of natural local seismicity, we implemented the stochastic test by using the same parameters, *i.e.*, the number of time steps, the number of earthquakes, and number of gridding boxes, of Fig. 3b to generate 500 artificial random seismic catalogues. An artificial catalogue was generated by using the same total number of earthquakes, assigning occurrence times from a uniform probability distribution from 1987 to 2009, and then distributing the earthquakes in each time step with uniform probability over the research region. Randomizing the catalogue in this way destroyed any inherent space-time structure, *e.g.*, the main shock-aftershock sequences, earthquake clusters, and induced earthquakes, which possibly existed in the original CWBSN catalogue. We performed the time series of inverse normalized TM metric for each artificial catalogue and calculated its correlation coefficient (Hoel 1966) with the result in Fig. 3b. We also generated another set of random catalogues by using the parameters of Fig. 3c and calculated their correlation coefficients with the result in Fig. 3c. Figure 6a, c shows the correlation coefficients relative to Fig. 3b-c, respectively. Figure 6b and d illustrates three inverse TM metric curves of random catalogues which correspond to the top three correlation coefficient values in Fig. 6a and c, respectively. The most immediate characteristic is that these curves merely have small fluctuations, instead of large drops observed in

Fig. 3b or c. In Figures 2b, 3b-c, and 4b, we observe that several candidates of effectively ergodic intervals are terminated by big drops. We suggest that the participation of enormous number of aftershocks temporally clustered in successive unit time steps obviously changed the stable distribution of long-term average seismic rate evaluated from previous seismicity. This iterative process of formation and sudden termination of effective ergodicity is similar to the researches using other natural catalogues such as of California, Spain, and eastern Canada (Tiampo *et al*. 2007).

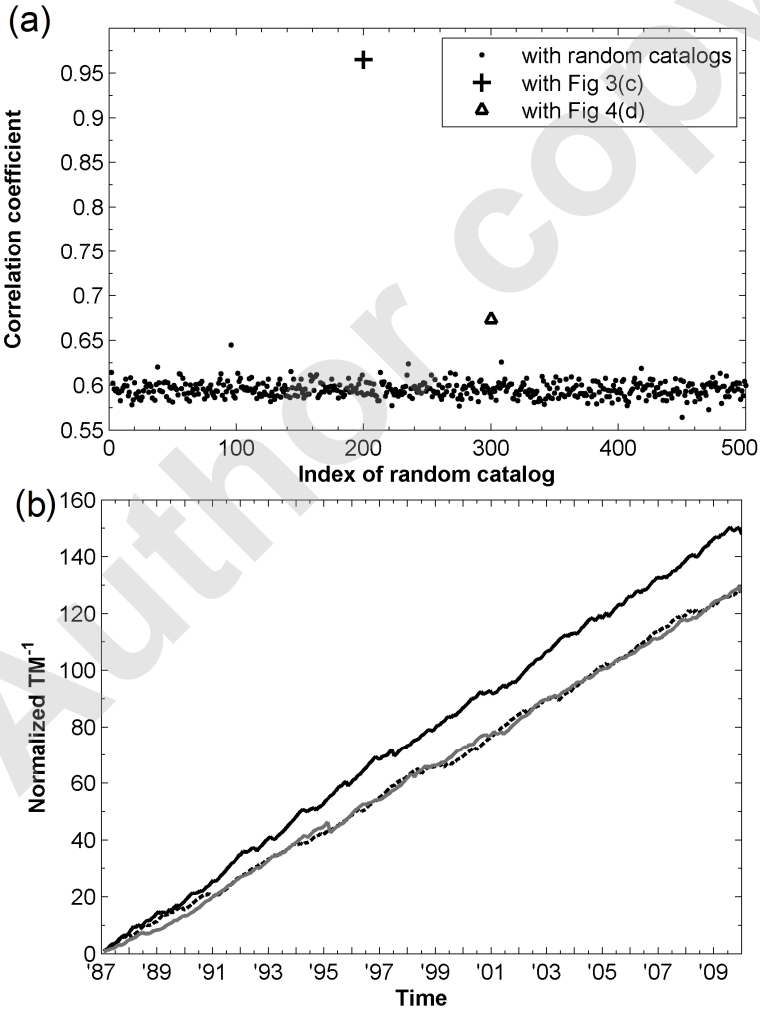

Fig. 6. Continued on next page.

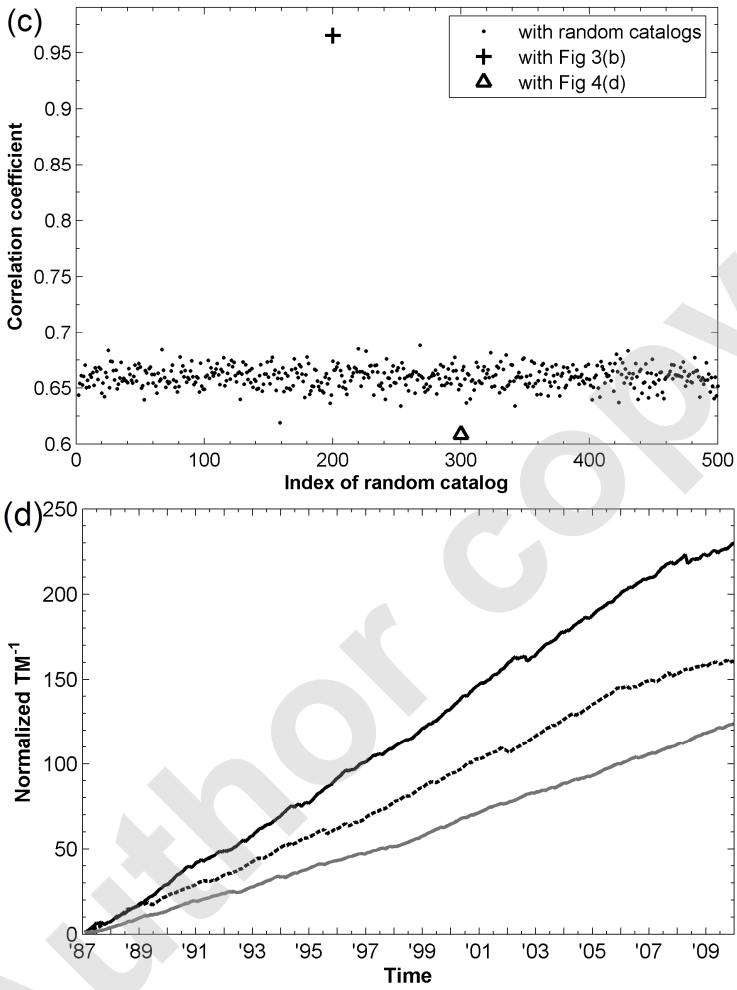

Fig. 6. Correlation coefficients of normalized inverse TM metric curves. Panel (a): cross refers to Fig. 3b and c, open triangle to Figs. 3b and 4d, and black dots to Fig. 3b and random catalogues. Panel (c): cross refers to Fig. 3c and b, open triangle to Figs 3c and 4d, and black dots to Fig. 3c and random catalogues. For (a) and (c), top three normalized inverse TM metric curves which have the highest correlation coefficients are shown in (b) and (d), respectively.

To illustrate the availability of correlation coefficient in distinguishing different patterns of inverse TM metric curves, we calculated the correlation coefficients for each pair of Figs. 3b-c and 4d. With visual inspection, the patterns of inverse TM metric curve are similar between Fig. 3b and c, but are quite different in 1987 to 1991 between Figs. 3b and 4d, and between

Figs. 3c and 4d. The cross in Fig. 6a and c indicates the value of correlation coefficient, amounting to 0.965, between Fig. 3b and c. The open triangles in Fig. 6a and c respectively, indicate the values of correlation coefficient between Figs. 3b and 4d, and between Figs. 3c and 4d. The value is 0.674 in Fig. 6a and 0.609 in Fig. 6c. With the interpretation developed by Dawson and Trapp (2004), values of correlation coefficient from 0.5 to 0.75 or from –0.5 to –0.75 indicate moderate to good correlation, and values from 0.75 to 1 or from –0.75 to –1 point to very good to excellent correlation between the variables. These apparent differences support the application of correlation coefficient as a simple but efficient statistical quantity to evaluate the similarity between patterns of inverse TM metric curve. The correlation coefficients ranged from 0.564 to 0.645 for each pair of Fig. 3b and random catalogues, and from 0.619 to 0.688 for the case of Fig. 3c. In both cases, the relatively lower values of correlation coefficient indicate that the patterns of inverse TM metric for random catalogues are quite different from Fig. 3b or c. The slopes of linear regression model for the curves in Fig. 6b are 0.541, 0.463, and 0.467, being 0.861, 0.605, and 0.446 for the curves in Fig. 6d. All slopes are much larger than those fitted by any candidate of effectively ergodic interval in Fig. 3b-c. Through the tests of correlation coefficient and fitted slope for randomized catalogues, we exclude the possibility that the big drops observed in Fig. 3b-c are generated occasionally due to parametric selection.

The Shapiro–Wilk test (Shapiro and Wilk 1965, Royston 1995) is applied to the candidates of effectively ergodic intervals in Figs. 3b-c, 4b, and the random catalogues in Fig. 6a, c to test if linear regression models are proper to simulate the behaviors of inverse TM metric in each case. The Shapiro–Wilk test is a widely used algorithm to test the null hypothesis that a sample came from a population with normal distribution. The Shapiro–Wilk test has better performance than the Kolmogorov–Smirnov (KS) test for testing for normality (Kvam and Vidakovic 2007). In our application, a sample is composed by the residuals of inverse normalized TM metric between simulated values obtained from linear regression model and values calculated from original data. According to the fundamental assumption of simple linear regression, the fitted regression model is adequate to describe the behaviors of a system once the residuals displays normal distribution (Cohen *et al.* 2003). We used two-side test and 0.05 as the significance level in our tests. In 500 random catalogues used in Fig. 6a, there are 439 catalogues the p values of which locate in the interval 0 to 0.05 (reject null hypothesis). In the random catalogues used in Fig. 6c, there are 446 catalogues the p value of which is under the predefined significance level. Briefly speaking, for over 90% of random catalogues in this analysis, the linear model is not suitable to describe the behaviors of inverse TM metric. The

p values of candidates of effectively ergodic interval are listed in Tables 1-4. Only the interval from July 1994 to August 1999, in Fig. 4b, has a relatively low *p* value comparing to other candidates, *i.e.*, 0.102. This low *p* value seems to correspond to stronger fluctuation of inverse normalized TM metric in the interval. On the other hand, most *p* values listed in Tables 1-4 are greater than the predefined significance level and support the adequacy of describing the behavior of normalized inverse TM metric curve by fitted linear regression model. Thus, we conclude that the statistical behaviors of long-term average seismicity can be regarded as effectively ergodic in several data sets selected from the CWBSN catalogue.

The identifications of effectively ergodic intervals in the CWBSN catalogue supports the researches in other natural seismic catalogues, such as of California, Spain, and eastern Canada. These analyses concluded that natural fault network displayed at least some of the dynamics of driven mean-field system, as observed in the numerical simulations of interacting slider block model and coupled map lattices. Ergodicity is a necessary condition to effectively use linear principal component analysis. The identified temporal and

Table 1

Slope of linear regression model and *p* value of Shapiro–Wilk test for Fig. 2b

Interval	1987/1-1990/4	1991/6-1994/5	1996/11-1999/8
Slope	0.627	0.158	0.029
p value	0.766	0.907	0.799

Table 2

Slope of linear regression model and *p* value of Shapiro–Wilk test for Fig. 3b

Interval	1991/6-1994/5	1994/8-1996/8	1996/11-1999/8	2000/9-2002/2	2005/6-2009/6
Slope	0.154	0.117	0.119	0.078	0.066
p value	0.916	0.886	0.690	0.912	0.866

Table 3

Slope of linear regression model and *p* value of Shapiro–Wilk test for Fig. 3c

Interval	1991/6-1994/5	1994/8-1996/8	1996/11-1999/8	2000/9-2002/2	2005/6-2009/6
Slope	0.199	0.181	0.190	0.131	0.118
p value	0.673	0.963	0.441	0.889	0.939

Table 4

Slope of linear regression model and *p* value of Shapiro–Wilk test for Fig. 4a

Interval	1991/6-1992/4	1992/8-1994/4	1994/7-1999/8
Slope	0.160	0.143	0.095
p value	0.756	0.607	0.102

spatial parameters which corresponded to effective ergodicity are critical for employing such linear approximation methods based on long term statistic quantity.

Acknowledgement. HCL is grateful for the support from the National Science Council (ROC) and the Institute of Geophysics, NCU (ROC). The work of CCC is supported by the National Science Council (ROC) and the Department of Earth Sciences, NCU (ROC). The authors thank Professor Kristy F. Tiampo (University of Western Ontario, Canada) for fundamental works and precious opinions of TM metric. The effort of Central Weather Bureau to maintain the CWBSN is highly appreciated.

References

Bak, P., C. Tang, and K. Weisenfield (1987), Self-organized criticality: An explanation of the 1/*f* noise, *Phys. Rev. Lett.* **59**, 4, 381-384, DOI: 10.1103/PhysRevLett.59.381.

Chen, C.-C., J.B. Rundle, J.R. Holliday, K.Z. Nanjo, D.L. Turcotte, S.C. Li, and K.F. Tiampo (2005), The 1999 Chi-Chi, Taiwan, earthquake as a typical example of seismic activation and quiescence, *Geophys. Res. Lett.* **32**, L22315, DOI: 10.1029/2005GL023991.

Chen, C.-C., J.B. Rundle, H.C. Li, J.R. Holliday, K.Z. Nanjo, D.L. Turcotte, and K.F. Tiampo (2006), From tornadoes to earthquakes: Forecast verification for binary events applied to the 1999 Chi-Chi, Taiwan, earthquake, *Terr. Atmos. Ocean. Sci*. **17**, 503-516.

Chen, C.-C., Y.-T. Lee, and L.-Y. Chiao (2008), Intermittent criticality in the long-range connective sandpile (LRCS) model, *Phys. Lett. A* **372**, 24, 4340-4343, DOI: 10.1016/j.physleta.2008.04.043.

Cohen, J., P. Cohen, S.G. West, and L.S. Aiken (2003), *Applied Multiple Regression Correlation Analysis for the Behavioral Sciences,* Lawrence Erlbaum Associates Inc., New Jersey.

Dawson, B., and R.G. Trapp (2004), *Basic and Clinical Biostatistics*, 4th ed., Lange Medical Books, McGraw-Hill, New York.

Ferguson, C.D., W. Klein, and J.B. Rundle (1999), Spinodals, scaling and ergodicity in a model of an earthquake fault with long-range stress transfer, *Phys. Rev. E* **60**, 1359-1373, DOI: 10.1103/PhysRevE.60.1359.

Fisher, D.S. (1985), Sliding charge-density waves as a dynamic critical phenomenon, *Phys. Rev. B* **31**, 3, 1396-1427, DOI: 10.1103/PhysRevB.31.1396.

Fisher, D.S., K. Dahmen, S. Ramanathan, and Y. Ben-Zion (1997), Statistics of earthquakes in simple models of heterogeneous faults, *Phys. Rev. Lett*. **78**, 25, 4885-4888, DOI: 10.1103/PhysRevLett.78.4885.

Gopal, A.D., and D.J. Durian (1995), Nonlinear bubble dynamics in a slowly driven foam, *Phys. Rev. Lett.* **75**, 2610-2613, DOI: 10.1103/PhysRevLett.75.2610.

Gutenberg, B., and C.F. Richter (1954), *Seismicity of the Earth and Associated Phenomena*, 2nd ed., Princeton University Press, New Jersey.

Habermann, R.E. (1987), Man-made changes of seismicity rates, *Bull. Seismol. Soc. Am*. **77**, 141-159.

Hertz, J., A. Korgh, and R.G. Palmer (1991), *Introduction to the Theory of Neural Computation*, Addison Wesley, Reading, MA.

Herz, A.V.M., and J.J. Hopfield (1995), Earthquake cycles and neural reverberations: Collective oscillations in systems with pulse-coupled threshold elements, *Phys. Rev. Lett*. **75**, 1222-1225, DOI: 10.1103/PhysRevLett.75.1222.

Hoel, P.G. (1966), *Introduction to Mathematical Statistics*, Wiley Series in Probability and Statistics, John Wiley & Sons, New York.

Klein, W., J.B. Rundle, and C.D. Ferguson (1997), Scaling and nucleation in models of earthquake faults, *Phys. Rev. Lett.* **78**, 19, 3793-3796, DOI: 10.1103/PhysRevLett.78.3793.

Kvam, P.H., and B. Vidakovic (2007), *Nonparametric Statistics with Applications to Science and Engineering*, John Wiley & Sons, New Jersey.

Lee, Y.-T., C.-C. Chen, Y.-F. Chang, and L.-Y. Chiao (2008), Precursory phenomena associated with large avalanches in long-range connective sandpile (LRCS) model, *Physica A* **387**, 21, 5263-5270, DOI: 10.1016/j.physa.2008.05.004.

Mignan, A., M.J. Werner, S. Wiemer, C.-C. Chen, and Y.-M. Wu (2011), Bayesian estimation of the spatially varying completeness magnitude of earthquake catalogs, *Bull. Seismol. Soc. Am*. **101**, 3, 1371-1385, DOI: 10.1785/0120100223.

Ogata, Y., and K. Katsura (1993), Analysis of temporal and spatial heterogeneity of magnitude frequency distribution inferred from earthquake catalogues, *Geophys. J. Int.* **113**, 727-738, DOI: 10.1111/j.1365-246X.1993.tb04663.x.

Royston, P. (1995), A remark on algorithm AS 181: the W-test for normality, *J. Roy. Stat. Soc., Ser. C* **44**, 4, 547-551.

Rundle, J.B., and W. Klein (1995), New ideas about the physics of earthquakes, *Rev. Geophys.* **33**, S1, 283-286, DOI: 10.1029/95RG00106.

Rundle, J.B., K.F. Tiampo, W. Klein, and J.S. Sá Martins (2002), Self-organization in leaky threshold systems: The influence of near-mean field dynamics and its implications for earthquakes, neurobiology, and forecasting, *Proc. Nat. Acad. Sci. USA* **99**, Suppl. 1, 2514-2521, DOI: 10.1073/pnas.012581899.

Scholz, C.H. (1990), The *Mechanics of Earthquakes and Faulting*, Cambridge University Press, Cambridge, UK.

Shapiro, S.S., and M.B. Wilk (1965), An analysis of variance test for normality (complete samples), *Biometrika* **52**, 3-4, 591-611.

Telesca, L., C.-C. Chen, and Y.-T. Lee (2009), Scaling behaviour in temporal fluctuations of crustal seismicity in Taiwan, *Nat. Hazards Earth Syst. Sci*. **9**, 2067-2071, DOI: 10.5194/nhess-9-2067-2009.

Thirumalai, D., R.D. Mountain, and T.R. Kirkpatrick (1989), Ergodic behavior in supercooled liquids and in glasses, *Phys. Rev. A* **39**, 7, 3563-3574, DOI: 10.1103/PhysRevA.39.3563.

Tiampo, K.F., J.B. Rundle, S. McGinnis, S.J. Gross, and W. Klein (2002), Mean-field threshold systems and phase dynamics: An application to earthquake fault systems, *Europhys. Lett.* **60**, 3, 481-487, DOI: 10.1209/epl/i2002-00289-y.

Tiampo, K.F., J.B. Rundle, W. Klein, J.S. Sá Martins, and C.D. Ferguson (2003), Ergodic dynamics in a natural threshold system, *Phys. Rev. Lett*. **91**, 238501, DOI: 10.1103/PhysRevLett.91.238501.

Tiampo, K.F., J.B. Rundle, W. Klein, J. Holliday, J.S. Sá Martins, and C.D. Ferguson (2007), Ergodicity in natural earthquake fault networks, *Phys. Rev. E* **75**, DOI: 10.1103/PhysRevE.75.066107.

Tiampo, K.F., W. Klein, H.-C. Li, A. Mignan, Y. Toya, S.Z.L. Kohen-Kadosh, J.B. Rundle, and C.-C. Chen (2010), Ergodicity and earthquake catalogs: Forecast testing and resulting implications, *Pure Appl. Geophys*. **167**, 6-7, 763-782, DOI: 10.1007/s00024-010-0076-2.

Tsai, C.-Y., G. Ouillon, and D. Sornette (2011), New empirical tests of the multifractal Omori law for Taiwan, *arXiv:1109.5017v1*.

Urbach, J.S., R.C. Madison, and J.T. Markert (1995), Interface depinning, self-organized criticality, and the Barkhausen effect, *Phys. Rev. Lett*. **75**, 2, 276-279, DOI: 10.1103/PhysRevLett.75.276.

Wiemer, S. (2001), A software package to analyze seismicity: ZMAP, *Seismol. Res. Lett*. **72**, 3, 373-382, DOI: 10.1785/gssrl.72.3.373.

Wiemer, S., and M. Wyss (2000), Minimum magnitude of completeness in earthquake catalogs: Examples from Alaska, the Western United States, and Japan, *Bull. Seismol. Soc. Am.* **90**, 4, 859-869, DOI: 10.1785/0119990114.

Wu, Y.-M., C.-C. Chen, L. Zhao, and C.-H. Chang (2008), Seismicity characteristics before the 2003 Chengkung, Taiwan, earthquake, *Tectonophysics* **457**, 177-182, DOI: /10.1016/j.tecto.2008.06.007.

Received 20 August 2011
Received in revised form 9 February 2012
Accepted 13 February 2012